18th International Conference on Ships and Shipping Research 2015, June 24th – 26th, Lecco, Italy

M. Altosole and A. Francescutto (Editors)

NUMERICAL AND EXPERIMENTAL INVESTIGATION ON THE WAVE-WAVE INTERACTION IN BREAKING AND NON-BREAKING FOCUSING WAVES

Guido LUPIERI [1], Thomas PUZZER [1], Giorgio CONTENTO [1], Luca DONATINI [1], Lorenzo CAPPIETTI [2]

[1] HyMOLab - Dept. of Engineering and Architecture – University of Trieste, Trieste, Italy, corresponding author: glupieri@units.it

[2] LABIMA - Dept. of Civil and Environmental Engineering – University of Florence, Florence, Italy, lorenzo.cappietti@unifi.it

ABSTRACT

The modelling of large individual waves for the computation of loads on ships and offshore structures in extreme weather conditions is still a challenging problem. Since the early 50s the predictions of loads on fixed offshore structures and motions of compliant or sailing structures due to surface waves are commonly made by computations on the basis of the statistical/spectral description of the sea elevation and of a linearized response model. Quadratic Transfer Functions or fully non-linear methods are used only in specific cases. The linear approach is recognized to work reasonably well for the so-called operational conditions, assuming that hydrodynamic and dynamic nonlinear effects can be neglected. On the other hand, it is also recognized that the modelling of large amplitude motions and the modelling of waves in the so-called survival conditions, i.e. extreme wave conditions, cannot recast a linear approach. In these conditions the wave-wave interaction plays a fundamental role (energy transfer, down-shift, etc) in the actual deterministic or spectral representation of the wave/flow field and thus in the related loads on the structure.
In the present paper the nonlinear aspects related to the behavior of steep focusing breaking and non-breaking waves are analyzed by means of numerical simulations and new experiments. The experiments are carried out at the wave flume of the Laboratory of Maritime Engineering (LABIMA) of the Dept. of Civil and Environmental Engineering of the University of Florence. The computations are carried out at Hydrodynamic and MetOcean Laboratory (HyMO*Lab*) of the Dept. of Engineering and Architecture of the University of Trieste. The paper focuses the attention on the comparison between the results obtained with a state-of-art viscous flow simulation and laboratory experiments, with particular emphasis on the spectral energy exchange between component waves of a non-breaking and breaking focusing wave train. This study is carried out as part of the research project “OpenViewSHIP Development of an integrated computational ecosystem for the hydrodynamic design of the hull-propeller system”, co-financed by Friuli Venezia Giulia Region in the field of industrial application of open-source CFD and High Performance Computing.

1. INTRODUCTION

The nonlinear nature of steep - even non breaking - waves is a very important subject of research in the Naval Architecture field as well as in the more general Marine Hydrodynamics field. Among others, it regards the interaction of the fluid with the sea bed in the shoaling region (see for instance Lubin et al., 2011), the interaction of the fluid with bodies close to the free surface in steady or unsteady mode (see for instance Contento and Codiglia, 2001), the self-

ISBN 978-88-940557-1-9

interaction of harmonic components of steep waves even in deep water (see for instance Chaplin, 1996) and the stability of steep regular wave trains (Benjamin-Feir, 1967).
In particular the modelling of large individual waves for the computation of loads on ships and offshore structures in extreme weather conditions is still a challenging problem. The phase averaged spectral description of the sea elevation is now an almost common procedure. It is based on the superposition of linear wave components and this implies (pros&cons) the superposition of the associated kinematics, induced pressures, dynamics, motions, structural response and so on. The computational advantages related to the assumption of linearity are enormous so that the method is widely accepted, mostly for the so-called operational conditions. On the other hand, it is also recognized that the predictions of large amplitude motions or loads/motions in the so-called survival conditions, typically a single (design) wave with a very low occurrence probability, cannot recast a linear phase averaged approach. These environmental conditions derive from an unlucky superposition of wave components, namely when the maximum elevation of the components within the relevant part of the sea spectrum are almost in phase (focusing) in a specific place, leading to the so-called freak waves. The experimental evidence of these events at sea is getting wider and wider (among others Clauss, 1999; Myrhaug and Kieldsen, 1986; http://en.wikipedia.org/wiki/Draupner_wave, Swan, 2014; http://www.glerl.noaa.gov/res/Task_rpts/2002/ppliu02-3.html).
Limiting the analysis to the wave-wave interaction of component waves in a focusing wave train, Chaplin (1996,1997) has shown by experimental tests in a lab that focused component waves behave in a fully non-linear manner in a relatively small region around the concentration point. In his experiments the maximum wave elevation is underestimated by linear predictions by 10% approximately, a non-negligible amount of energy is (not permanently) shifted to the high frequency range, well above the input spectrum, and at these new frequency components the phase speed shows an almost constant value.
Contento et al. (2001,2003) have investigated the focusing of non-breaking waves by time-domain fully-nonlinear numerical simulations in the frame of inviscid flow hypotheses. In those works the agreement with the experimental data of Chaplin (1996) was excellent. The shift of energy at high frequencies was well evidenced as well as the strongly non-linear behavior of the phase speed of the locked bound waves. The main limitation of that study, two-dimensionality apart, was the inviscid flow assumption that limited the further investigation on focusing breaking waves.
In this work, we overcome those limitations adopting a viscous flow approach with a Volume Of Fluid (Hirt and Nichols, 1981) technique that allows the simulation of strong wave breaking, including air entrapment. We still keep a two dimensional problem both to reduce the computational effort and mostly to focus on the nonlinear effects at focusing/breaking that had been already discussed in previous studies.
New experimental data presented here have been obtained recently at the wave flume of the Laboratory of Maritime Engineering of the Dept. of Civil and Environmental Engineering of the University of Florence.
The paper is organized as follows: the methods adopted to generate and analyze focusing waves in a physical or 2D numerical lab are described first, a brief description of the experimental tests/apparatus and of the mathematical/numerical model is given, finally the experimental and numerical results are discussed thoroughly, with concluding remarks.

2. GENERATION OF FOCUSING WAVES IN A BASIN AND DATA WINDOWING

Chaplin (1996) has given an overview of the three basic methods used in laboratories to obtain a concentration of energy at a specified station along a basin (focusing). Contento et al. (2001) have revised these methods so they will be not reported here again. Besides the technique used for focusing waves, undesired sources of disturbance in a wave record can make the identification of the actual nonlinear effects in the generated wave train difficult, polluting the solution. Thus they must be minimized whenever possible.
In this work we have adopted a new strategy (accurate data windowing) in order to make the time record at and around the focusing point clean, as much as possible.

ISBN 978-88-940557-1-9

The driving signal $\alpha(t)$ of the wave-maker is derived according to the wave-maker linear theory (Dean and Dalrymple, 1984), with the superposition of N_f harmonics of amplitude α_{0_i}, period T_i and angular frequency ω_i , as follows

$$\alpha(t) = \sum_{i=1}^{N_f} \alpha_i\,(t) = \sum_{i=1}^{N_f} \alpha_{0_i} \sin\,(\omega_i t - \varphi_i) \tag{1}$$

with $\omega_1 < \omega_2 < \cdots < \omega_{N_f}$.
In this case, the expected asymptotic behaviour of the outgoing wave is:

$$\eta(x,t) = \sum_{i=1}^{N_f} \frac{H_i}{2} \cos\,(k_i x - \omega_i t + \varphi_i) \tag{2}$$

The origin of the frame of reference is set at the calm water level at the mean position of the wave-maker $x = 0$, both for experiments and numerical simulations.
It is well known that there are several sources of disturbance to the wave train of Eq. 2, even in the linear case:

a) evanescent modes of decreasing amplitude occur close to the wavemaker, their amplitude and wave-number being related to the outgoing wave-number k_i and the relative water depth;
b) starting the wave-maker from the still water condition, the wave amplitude envelope moves with the wave group velocity c_{g_i} and it exhibits an oscillatory behaviour mostly close to the front of the wave train, i.e. the wave amplitude is not steady in space and time; in this implementation we allow 2 additional wave periods ($\delta_i = 2\,T_i$) before considering the wave train in steady condition after its theoretical front;
c) when the paddle is switched-on abruptly, low frequency fast waves are unavoidably generated so that transient effects in the wave front of each frequency component become even more complex than in b), both in time and space; to reduce this undesired effect, the paddle motion (Eq. 1) can be modified introducing a smooth ramp function:

$$\alpha_i(t) = \begin{cases} 0 & 0 \le t \le t_{start_i} \\ \frac{\alpha_{0_i}}{2}\left[\left(1 - \cos\,(\pi \frac{t - t_{start_i}}{\tau_i})\right) \sin\,(\omega_i t - \varphi_i)\right] & t_{start_i} \le t \le t_{start_i} + \tau_i \\ \alpha_{0_i} \sin(\omega_i t) & t_{start_i} + \tau_i \le t \end{cases} \tag{3}$$

   In this implementation $\tau_i = 2\,T_i$, i.e. twice the component wave period;
d) if the absorbing beach doesn't work properly, a very long computationally inefficient tank or alternatively a relatively short time window must be used;
e) sloshing modes of the closed basin are unavoidably activated by the wave-maker motion.

According to the positions above, the clean part of a wave train generated from the still water condition is here meant as the tail of the wave train after the virtual wave front given by the wave group velocity, adding the double delay introduced in items b) and c) above, i.e. δ_i and τ_i. Moreover this tail is here cut in correspondence of the virtual front of the reflected waves. The disturbances a) to e) can make the identification of the actual nonlinear effects of the generated wave train difficult. In the present work (both experimental and numerical), the main idea to prevent the loss of cleanliness of the wave train is to generate the component waves so that their own front has crossed the focusing station at the desired time with a specified minimum number of wave-lengths/wave-periods. In the following, the explanation of the method used is given. Please refer to Figure 1 for the explanation of the following.
The theoretical focusing at a given position x_{focus} along the tank of N_f regular waves of different wavelength is here defined as the condition for which all wave components in Eq. 2 show a crest at the position x_{focus} at a given time t_{focus}.
In this work, the frequencies of the component waves in Eq. 1 to 3 are chosen as multiple of a base frequency ω_0 (that not necessarily belongs to the input spectrum), i.e. $\omega_i = k \cdot \omega_0$, with $k_{min} \le k \le k_{max}$. In this way, whatever k_{min}, k_{max} are, the overall theoretical periodicity of the signal is $P = {}^{2\pi}/_{\omega_0}$. P corresponds to the length of the time-window over which the analysis will

ISBN 978-88-940557-1-9

be conducted at any position x along the tank, ensuring accuracy in the Fourier analysis. It is assumed here that at x_{focus} wave focussing will occur approximately at $^{P}/_{3}$.
In the present implementation $P = 25\ s$ and $k_{min} = 18, k_{max} = 34$.
Once x_{focus} has been fixed (in our case $x_{focus} = 7\ m$), the space-window over which the analysis will be conducted can prescribed. The starting and end points of the space-window are x_1 and x_2 respectively.
In this specific implementation we have adopted $(x_2 - x_{focus}) = 2 \cdot (x_{focus} - x_1)$.
Each line in Figure 1 corresponds to the wave group velocity c_{g_i} of each frequency component of the input spectrum. The lower bundle of lines represents the loci of the individual clean wave front in the direction of propagation, i.e. with the delay $\delta_i + \tau_i$. The upper bundle represents the theoretical loci (without delay $\delta_i + \tau_i$) of the individual wave front in the opposite direction of propagation (front of the reflected waves).
At x_1 the time-window P starts at time t_1 given by:

$$t_1 = max\left\{\left[max_i\left(\frac{x_1}{c_{g_i}} + \delta_i + \tau_i\right)\right], \left[max_i\left(\frac{x_2}{c_{g_i}} + \delta_i + \tau_i\right) - (x_2 - x_1)/c_{N_f}\right]\right\} \tag{4}$$

where c_{N_f} is the phase speed of the slowest wave component in the spectrum.
Analogously for t_2:

$$t_2 = max\left\{\left[max_i\left(\frac{x_2}{c_{g_i}} + \delta_i + \tau_i\right)\right], \left[max_i\left(\frac{x_1}{c_{g_i}} + \delta_i + \tau_i\right) + (x_2 - x_1)/c_{N_f}\right]\right\} \tag{5.1}$$

or

$$t_2 = t_1 + (x_2 - x_1)/c_{N_f} \tag{5.2}$$

Thus the grey parallelogram in Figure 1 corresponds to the space-time window where the wave elevation is expected to be free from disturbances (items a) – d) above) for $x_1 \le x \le x_2$. The time length or height of the parallelogram corresponds to the periodicity P. The slope of the parallelogram corresponds to $^{1}/_{c_{N_f}}$.
Finally, t_{focus} is given by:

$$t_{focus} = t_1 + \left(x_{focus} - x_1\right)/c_{N_f} + \left\{int\left[P/(3 \cdot T_{N_f})\right] \cdot T_{N_f}\right\} \tag{6}$$

For the specific spectrum considered here, it corresponds to $t_{focus} \approx 30\ s$.
Thus in Eq. 1 to 3, the following phases hold:

$$\varphi_i = \omega_i \cdot t_{focus} - k_i \cdot x_{focus} \tag{7}$$

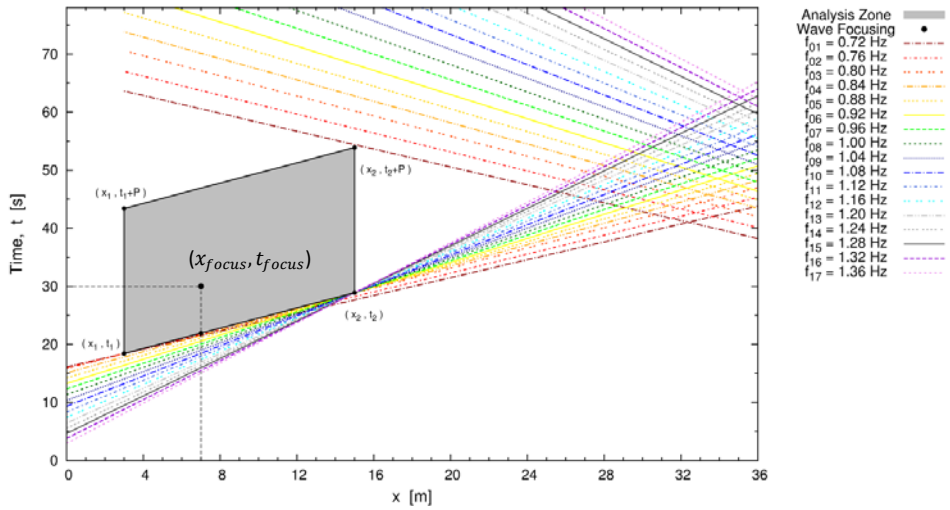

Figure 1. Space-time window for the frequency analysis

ISBN 978-88-940557-1-9

The experiments and simulations presented here refer to an input amplitude spectrum such that every frequency component has the same theoretical steepness $\left(H/\lambda\right)_i = const$. The selected amplitude spectra are $\left(H/\lambda\right)_i = \frac{1}{300}, \frac{1}{200}$, corresponding to a non-breaking and weakly breaking focusing event respectively.
Eqs. 1 to 7 hold under the linear hypothesis. Once the experiment or simulation has been done (nonlinear real case) and the component waves have been found to be not perfectly in phase at x_{focus}, the experiment or the simulation can be repeated updating the phase lag in Eq. 3, adding the perturbation phase derived from the first run. The method has shown a reasonable convergence (Contento et al., 2001) even with a single further phase-lag refinement step.

3. DESCRIPTION OF THE EXPERIMENTAL FACILITY AND SET-UP DETAILS

The wave-current flume of the LABIMA – Laboratory of Maritime Engineering, Dept. of Civil and Environmental Engineering of the University of Florence is $37\ m$ long, $0.8\ m$ wide and $0.8\ m$ high. The water depth was set to $0.50\ m$ during these experiments. The flume is equipped also with a water recirculation system that can generate a flow discharge up to $0.100\ m^3/s$ but it was turned off during these tests.
The wavemaker is of piston type, driven by an electro mechanic linear actuator with a maximum displacement of $0.150\ m$, maximum velocity $2\ m/s$ and maximum acceleration $2\ m/s^2$. The wave maker displacement is controlled by a servo-amplifier and a absolute encoder assuring an accuracy of $0.1\ mm$ in the positioning. The Biésel transfer function (Dean and Dalrymple, 1984) is used in order to compute the paddle motion trajectory as a function of the target wave conditions. The final transfer function has been obtained by experimental test with regular waves.
The used wave gauges are of ultrasonic type, Honeywell 943 series, with a declared repeatability $\pm\ 1\ mm$ that was experimentally confirmed. The sensors have measured well the focused waves without breaking $\left(H/\lambda\right)_i = \frac{1}{300}$. However, in case of wave breaking $\left(H/\lambda\right)_i = \frac{1}{200}$ the focused wave was so steep that the crest curvature and local wave slope overpassed the capability of the ultrasonic sensor; in those cases the measurement of the wave elevation was not complete. For this reason some results are not shown in this paper and those shown must be considered as a preliminary step towards new measurements. The use of new wave gauges has been planned for a new set of experiments in order to obtain good measurement also for such steep waves.
The experiments have been designed in order to fulfill the requirements given by Eqs. 1 to 7, as summarized in Fig. 1. The focusing station has been set to $x_{focus} = 7\ m$. The wave gauges have been positioned at $x_{wg1} = 3.0\ m$, $x_{wg2} = 5.0\ m$, $x_{wg3} = x_{focus} = 7.0\ m$, $x_{wg4} = 9.0\ m$, $x_{wg5} = 11.0\ m$, $x_{wg6} = 13.0\ m$ and $x_{wg7} = 15.0\ m$. The tests were repeated 4 times for each realization and each time the wave gauge array was shifted of $0.25\ m$ in order to obtain measurements with a space resolution of $0.25\ m$ along the basin. The measurements were collected with a sampling frequency of $20\ Hz$.

4. MATHEMATICAL / NUMERICAL MODELS AND SET-UP OF THE SIMULATIONS

Without heat exchanges, the governing equations in differential form for an incompressible Newtonian fluid are the following:

$$\frac{\partial(\rho u_i)}{\partial t} + \frac{\partial(\rho u_i u_j)}{\partial x_j} = -\frac{\partial p}{\partial x_i} + \frac{\partial}{\partial x_j}\left(\mu\left(\frac{\partial u_i}{\partial x_j} + \frac{\partial u_j}{\partial x_i}\right)\right) + F_i \qquad (8)$$

$$\frac{\partial u_i}{\partial x_i} = 0$$

ISBN 978-88-940557-1-9

where ρ is the fluid density, u_i is the velocity component, p is the pressure, μ is the dynamic viscosity, F_i is the body force, t and x_i are the time/space independent variables.
Broadly speaking, for small Reynolds numbers, the Navier-Stokes equations can be solved directly without any turbulence parameterization. When this modelling becomes necessary, among others, the RANSE approach can be used, based on the reformulation of the equations above in terms of Reynolds averages. Then, the closure of the new set of equations is achieved adding other equations in order that redefine the eddy viscosity.
In this work, the turbulence model in use (only when activated) is the Menter's k-ω Shear Stress Transport (1994) that consists of two extra transport equations: for the turbulent kinetic energy k and for a turbulence variable ω, namely function of dissipation and turbulent kinetic energy. As a general comment, the results obtained with a RANSE approach are not always satisfactory, especially in a transient regime and/or in specific confined zones. This limitation is due to many reasons as thoroughly discussed also in Lubin et al. (2006), Lubin et al. (2011) and Kimmoun and Branger (2007).
On the other hand, at industrial level, the simulation of the free surface flow around a ship hull even in model scale, with or without incident waves, is generally performed with a RANSE approach. The quality of the solution achieved should be known apriori at a design level, i.e. before coinductiong the experimental tests in the towing tank. The development of a robust computational framework for the production of affordable results in these topics is among the goals of the ongoing research work (Open*View*SHIP Project).
Being interested in two phase flows (a coupled air-water interface system), it is possible to deal with interface capturing methods as VOF technique by Hirt and Nichols (1981) in which a scalar indicator function α is used to represent the phase of the fluid in each cell. At the free surface the scalar α jumps from 1 to 0 and vice-versa over an extremely small distance. This feature can be associated to large gradients and therefore it becomes difficult to approximate the step-like nature of α at the free surface, unless a specific treatment of the equation for α is introduced (Rusche, 2002; Maki, 2011). The latter method has been used in this work.
The equations are solved over a finite volume (www.openfoam.org/docs/user/) using the following schemes, based on a 2nd order Gaussian integration as summarized in Table 1.

Table 1

Term		Discretization
Gradient	∇	linear
Convection	$\nabla \cdot (\rho\phi U)$	limited linearV 1
	$\nabla \cdot (\phi\alpha)$	vanLeer
	$\nabla \cdot (\phi_{rh}\alpha)$	interfaceCompression
Laplacian	$\nabla^2\phi$	linear corrected

The pressure-velocity coupling is achieved using a PISO algorithm. Euler explicit scheme is adopted to march forward in time. The free-surface location is computed using the multidimensional universal limited for explicit solution (MULES) method.
The computational domain reproduces exactly the dimensions of the experimental laboratory. The grid adopted has 664345 cells for non-breaking focusing wave with a resolution of approximately 120 cells per wave height and 200 per wave length, 3033040 cells for breaking focusing wave with a resolution of approximately 240 cells per wave height and 400 per wave length, 4x3 blocks with grading, with a refinement region around x_{focus}.

5. RESULTS AND DISCUSSION

5.1 Non-breaking wave focusing

Fig. 2a-b shows the time records of the free surface elevation at x_{focus} for the non-breaking case $\left(H/\lambda\right)_i = \frac{1}{300}$, without (a) and with (b) phase lag refinement, experimental (red line), numerical (blue line) and linear model (dotted black line). Fig. 3a-b shows the corresponding phase over the periodicity window P at x_{focus} (see Fig. 1) before (a) and after (b) the phase lag refinement.

ISBN 978-88-940557-1-9

The differences between the experimental and the numerical wave elevation before the phase lag refinement (Fig. 2a) are probably due to the different wavemaking method (moving piston Vs prescribed velocities at a fixed boundary). Fig. 3a shows evident differences between the attained phase in the experiments and in the simulations before the phase lag refinement. After the refinement, the comparison between the theoretical, experimental and numerical phases (Fig. 3b) is excellent and the comparison between the experimental and the numerical wave elevation is very good too (Fig. 2b). From both Figures 2a and 2b, it is clear how a small difference in the phase between wave component induces large differences in the wave elevation, specifically at the previous and following crest and troughs, demonstrating the complexity of the simulated or measured phenomenon.
Fig. 4a,d shows the time record and the corresponding amplitude spectrum of the free surface elevation at $x_{wg1}, x_{focus}, x_{wg5}, x_{wg7}$, with phase lag refinement. The comparison between experimental and numerical results is very good, both in time and in frequency domain. As expected, in this case $\left(H/\lambda\right)_i = \frac{1}{300}$ the change of the shape of the spectrum with space x is rather small because of the relatively low steepness of the focused wave profile ($\left(H/\lambda\right)_{focus} \cong \frac{1}{28}$).
However, the wave-wave interaction generates bound waves at frequencies higher and lower than the input spectrum. In both experiments and simulations there is a modulation of the amplitude of frequencies higher than the input band. This modulation is progressively compressed towards the input band, with increasing x. Moreover there is a remarkable growth with x of the lowest frequency components. This behavior had been already observed by Chaplin (experimental) (1996) and by Contento et al. (numerical) (2001,2003). Fig. 5 shows the contour plot of the amplitude spectrum along the tank. The bound waves induced by the wave-wave interaction is well visible, especially at frequencies higher and lower than the input band.
Fig. 6 shows a snapshot at $t \cong t_{focus}$ of the free surface with superposed the numerical result at $t = t_{focus}$. For sake of completeness, Fig. 7a,d shows the free surface profiles for a sequence of equally spaced time steps (every 0.5 s), including $t = t_{focus}$, experimental (red symbols), numerical without (light blue) and with phase lag (dark blue) refinement and linear model (dotted line). Again the comparison between experimental and numerical results is very good.

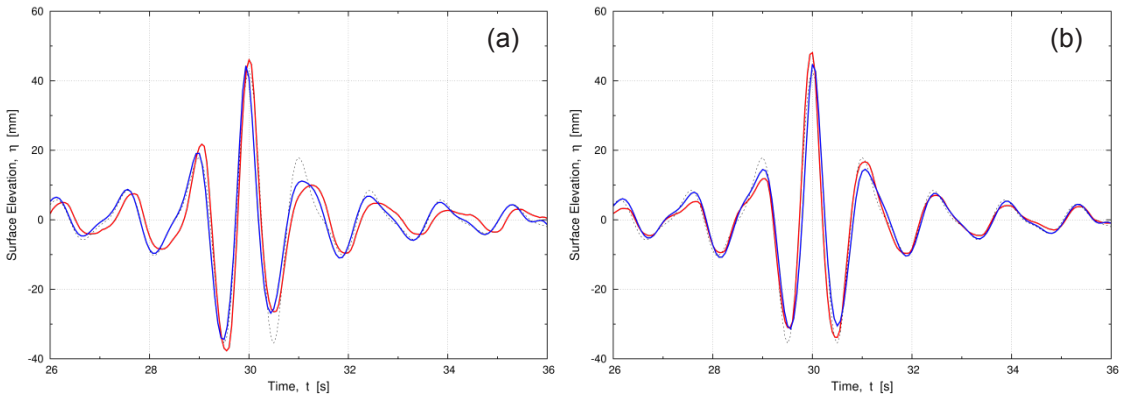

Fig. 2a,b - Time records of the free surface elevation at x_{focus} . $\left(H/\lambda\right)_i = \frac{1}{300}$, without (a) or with(b) phase lag refinement, experimental (——), numerical (——) and linear model (·····).

ISBN 978-88-940557-1-9

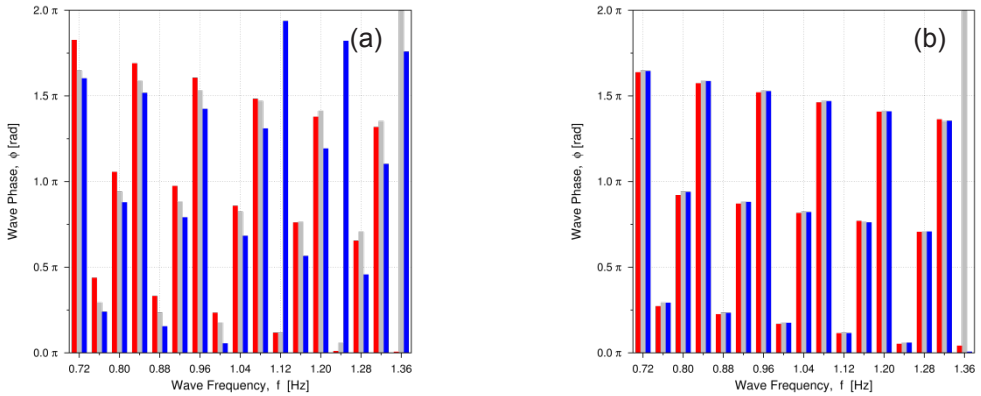

Fig. 3a,b – Phase of the component waves over the periodicity window P at x_{focus} (see Fig. 1). $\left(H/\lambda\right)_i = \frac{1}{300}$ before (a) and after (b) the phase lag refinement, experimental ( ), numerical ( ), linear model ( ).

5.2 Breaking wave focusing

The steepness of the component waves is now set to $\left(H/\lambda\right)_i = \frac{1}{200}$. In this case the change of the shape of the spectrum with space x is expected to be large.

Fig. 8a,d shows the time record and the corresponding amplitude spectrum of the free surface elevation at $x_{wg1}, x_{focus}, x_{wg5}, x_{wg7}$, with phase lag refinement.

As explained in §3, the measurement of the wave elevation at x_{focus} was affected by a systematic error of the ultrasonic gauge, due to the large slope and wave crest curvature. Fig. 8b shows this rather evidently. For this reason, the corresponding amplitude spectrum of the experimental data is not plotted.

In Fig. 8c the second wave crest is cut too and the amplitude spectrum shows an evident cut at upper frequencies of the input band. Due to this insurmountable technical problem, the entire measurement was affected by a large uncertainty and specifically the phase lag refinement could not be performed with full care. Anyway, Fig. 9 shows the contour plot of the amplitude spectrum along the basin. In this case, the strong wave-wave interaction is witnessed by the presence of large amplitude harmonics well outside the input band, with larger amplitudes close to the focusing station. As above, there is a kind of modulation of the amplitude of frequencies higher than the input band. This modulation is progressively compressed towards the input band with increasing x. Moreover there is a strong peak at the lowest frequency components around and after x_{focus}. In addition, within the input band, the amplitudes in the upper part are largely eroded around x_{focus}, as witnessed also by Fig. 8b,c,d.

However, the simulated focusing wave does not break, as shown in Fig. 10. This is undoubtedly due to the missing accurate phase-lag refinement and possibly to a not aligned performance of the wavemaking boundary compared to the physical wavemaker (left to a further calibration, both numerical and experimental).

ISBN 978-88-940557-1-9

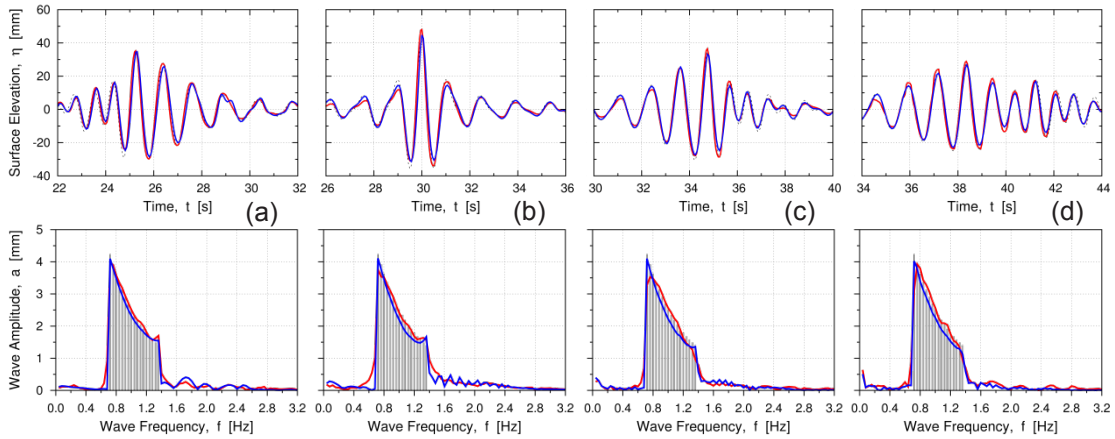

Fig. 4a,d – Time records and corresponding amplitude spectrum of the free surface elevation at $x_{wg1}\,(a), x_{focus}(b), x_{wg5}(c), x_{wg7}(d)$. $\left(H/\lambda\right)_i = \frac{1}{300}$, with phase lag refinement, experimental (——), numerical (——), linear model (——).

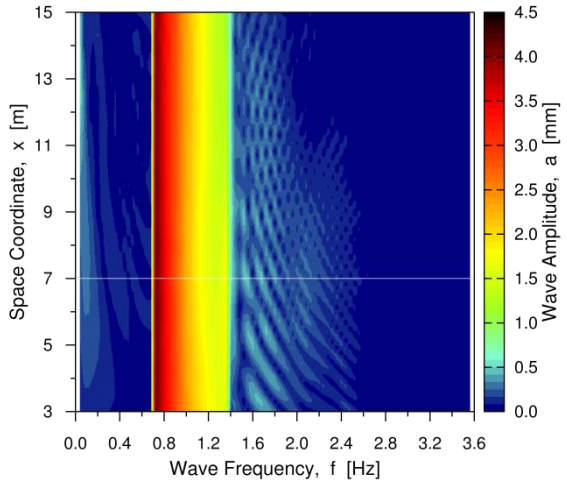

Fig. 5 – Amplitude spectrum of the free surface elevation along the tank, with phase lag refinement. $\left(H/\lambda\right)_i = \frac{1}{300}$.

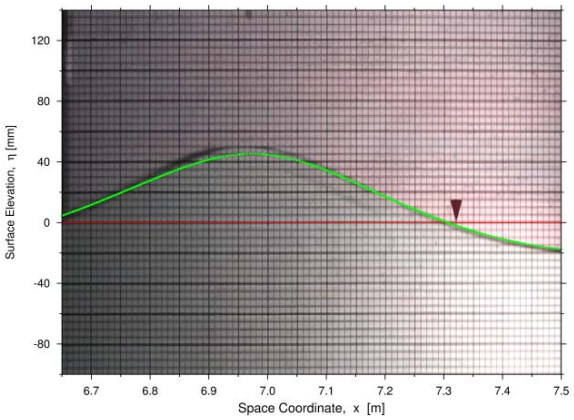

Fig. 6 – Snapshot of the free surface profile at $t = t_{focus}$. $\left(H/\lambda\right)_i = \frac{1}{300}$ with phase lag refinement. Numerical (——).

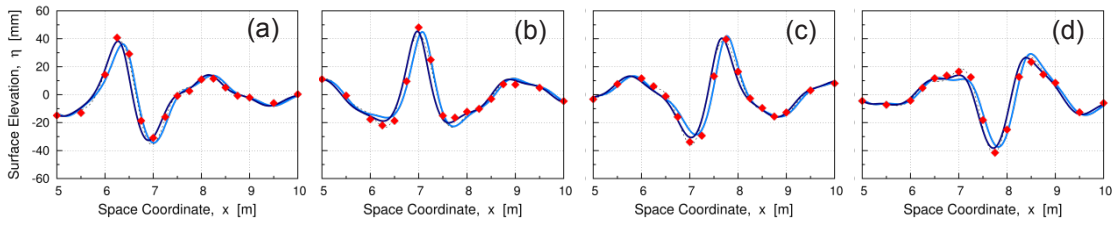

Fig. 7a,d – Free surface profiles at $t = t_{focus} - 0.5s$ (a), $t = t_{focus}$ (b), $t = t_{focus} + 0.5s$ (c) and $t = t_{focus} - 1.0s$ (d). $\left(H/\lambda\right)_i = \frac{1}{300}$. Experimental with phase lag refinement (◆), numerical with phase lag refinement (——), numerical without phase lag refinement (——), linear model (·····).

ISBN 978-88-940557-1-9

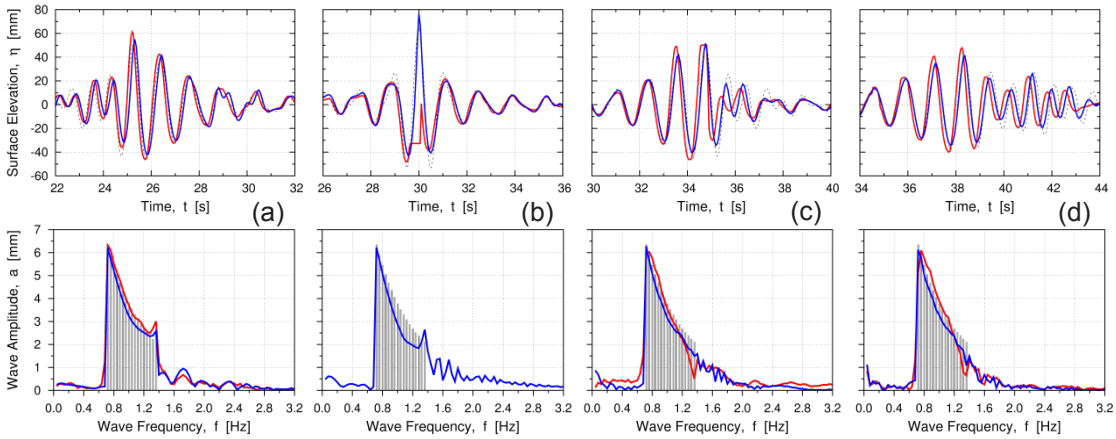

Fig. 8a,d – Time records and corresponding amplitude spectrum of the free surface elevation at $x_{wg1}, x_{focus}, x_{wg5}, x_{wg7}$. $\left(H/\lambda\right)_i = \frac{1}{200}$, with phase lag refinement, experimental (——), numerical (——), linear model (——).

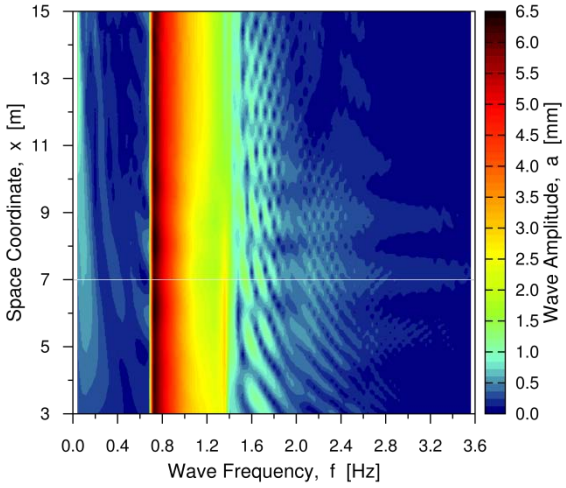

Fig. 9 – Amplitude spectrum of the free surface elevation along the tank, with phase lag refinement. $\left(H/\lambda\right)_i = \frac{1}{200}$

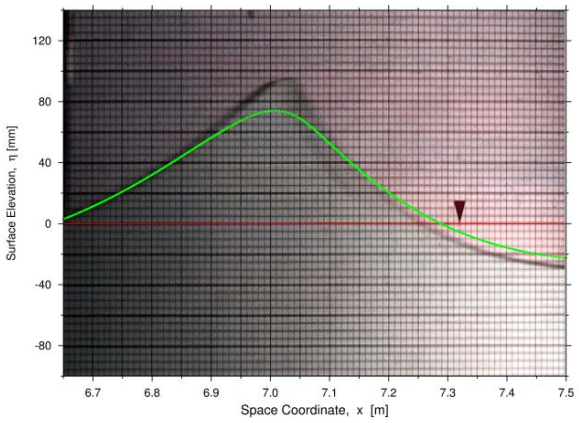

Fig. 10 – Snapshot of the free surface profile at $t = t_{focus}$. $\left(H/\lambda\right)_i = \frac{1}{200}$ with phase lag refinement. Numerical (——).

6. CONCLUSIONS

In this study the interaction between wave components in a given spectrum has been analysed by means of new experimental tests and viscous flow simulations. The investigation has highlighted the strong nonlinear behaviour of the wave-wave interaction at (or close to) focusing, with increasing complexity with the increasing wave steepness, mostly in terms of change of the shape of the spectrum (ergodicity assumption in linear theory). The analysis has shown the extremely good capabilities of the simulations to capture the core of the wave-wave interaction. On the other hand, the study has shown the need of an extremely accurate alignment of the wavemaking method between experiments and numerical simulations. Extremely small differences in the two transfer functions may lead to a strong difference in the wave profile at focusing. Further analysis is in progress on the flow field and energy loss, including the effect of turbulence and turbulence modelling in the breaking region.

ISBN 978-88-940557-1-9

AKNOWLEDEGMENTS

The “Programma Attuativo Regionale del Fondo per lo Sviluppo e la Coesione (PAR FSC) 2007–2013 - Linea d’Azione 3.1.2” is acknowledged for providing the financial support of the OpenViewSHIP Project.

REFERENCES

Benjamin, T.B.; Feir, J.E., 1967. "The disintegration of wave trains on deep water. Part 1. Theory". *Journal of Fluid Mechanics* Vol. 27 (3): 417–430.

Chaplin JR. 1996. On Frequency-Focusing Unidirectional Waves. *International Journal on Offshore and Polar Engineering*, 6(2): 131-137.

Chaplin JR, Rainey RCT, Yemm RW. 1997. Ringing of a vertical cylinder in waves. *Journal of Fluid Mechanics*, 350: 119-147.

Clauss GF. 1999. Task-related wave groups for seakeeping tests or simulation of design storm waves. *Applied Ocean Research*, 21: 219-234.

Contento, G., Codiglia, R., 2001, Nonlinear free surface induced pressure on a submerged horizontal circular cylinder at low Keulegan-Carpenter numbers, *International Journal Applied Ocean Research,* Vol. 23, pp. 175-185.

Contento, G., Codiglia, R., D’Este, F., 2001, Nonlinear effects in transient non-breaking waves in a closed flume, *Applied Ocean Research*, Vol. 23/1, pp. 3-13.

Contento, G., D’Este, F., Codiglia, R., 2003, Numerical Study on the Non-linear Behaviour of Steep Isolated Unidirectional Waves, *13rd International Conference on Offshore and Polar Engineering – ISOPE’2003*, May 2003, Honolulu – Hawaii, USA, Vol. 3, pp. 100-105.

Dean RG, Dalrymple RN. 1984. Water Wave Mechanics for Engineers and Scientists. World Scientific Advanced Series on Ocean Engineering, 1984, Prentice Hall Inc., Englewood Cliffs NJ.

Hirt C.W. and Nichols B.D. Volume of Fluid (VOF). 1981. Method for the Dynamics of Free Boundaries. *J. Comput. Phys,* Vol. 39, 201-225.

Kimmoun O. & Branger H., 2007. A particle image velocimetry investigation on laboratory surf-zone breaking waves over a sloping beach. *J. Fluid Mech.,* 588, 353-397.

Lubin P., Vincent S., Abadie S., Caltagirone J., 2006 Three-dimensional Large Eddy Simulation of air en- trainment under plunging breaking waves. *Coastal Engineering*, 53, 631-655.

Lubin, P., Glockner S., Kimmoun O., Branger H., 2011. Numerical study of the hydrodynamics of regular waves breaking on a sloping beach. *Eur. J. Mech. B/Fluids*, 30, 552-564.

Maki, K., 2011. Ship Resistance Simulations with OpenFOAM. 6th OpenFOAM Workshop, The Pennsylvania State University State College, PA, USA, 13-16 June.

Menter, F. R. 1994. Two-Equation Eddy-Viscosity Turbulence Models for Engineering Applications. *AIAA Journal*, No. 8, pp. 1598-1605, 1994.

Myrhaug D, Kieldsen SP. 1986. Steepness and Asymmetry of Extreme Waves and the Highest Waves in Deep Water. *Ocean Engineering*; 13(6): 549-568.

Rusche, H., 2002. Computational Fluid Dynamics of Dispersed Two - Phase Flows at High Phase Fractions. Imperial College of Science, Technology & Medicine, London.

http://en.wikipedia.org/wiki/Draupner_wave

http://www.openfoam.org/docs/user/

ISBN 978-88-940557-1-9